Data in Brief 21 (2018) 1435–1444

Contents lists available at ScienceDirect

Data in Brief

journal homepage: www.elsevier.com/locate/dib

Data Article

Supporting plots and tables on vapour–liquid equilibrium prediction for synthesis gas conversion using artificial neural networks

Precious Chukwuweike Eze, Cornelius Mduduzi Masuku *

Department of Civil and Chemical Engineering, University of South Africa, Private Bag X6, Florida, 1710, South Africa

A R T I C L E I N F O

Article history:
Received 17 October 2018
Received in revised form
21 October 2018
Accepted 25 October 2018
Available online 29 October 2018

Keywords:
Artificial neural networks
Fischer–Tropsch reaction
Machine learning
Thermodynamic modeling
Phase equilibrium

A B S T R A C T

This article contains data on vapor–liquid equilibrium modeling of 1533 gas-liquid solubilities divided over sixty binary systems viz. carbon monoxide, carbon dioxide, hydrogen, water, ethane, propane, pentane, hexane, methanol, ethanol, 1-propanol, 1-butanol, 1-pentanol, and 1-hexanol in the solvents phenanthrene, 1-hexadecanol, octacosane, hexadecane and tetraethylene glycol at pressures up to 5.5 MPa and temperatures from 293 to 553 K using literature data. The solvents are considered to be potentially significant in the conversion of synthesis gas through gas-slurry processes. Artificial neural networks limited to one hidden layer and up to five neurons in the hidden layer were used to predict the binary plots.

Specifications table

Subject area	*Chemical Engineering*
More specific subject area	*Thermodynamic Phase Equilibria*
Type of data	*Tables, and Figures*
How data was acquired	*Generated through a code on MATLAB®*

DOI of original article: https://doi.org/10.1016/j.sajce.2018.10.001
* Corresponding author.
E-mail address: masukcm@unisa.ac.za (C.M. Masuku).

https://doi.org/10.1016/j.dib.2018.10.129

Data format	*Filtered*
Experimental factors	*Feature scaling*
Experimental features	*Code was implemented on MATLAB®*
Data source location	*Input experimental data was obtained from* Breman et al. (1994).
Data accessibility	*Source data is available on Journal of Chemical & Engineering Data:* https://pubs.acs.org/doi/abs/10.1021/je00016a004
Related research article	P.C. Eze, C.M. Masuku, Vapour–Liquid Equilibrium Prediction for Synthesis Gas Conversion using Artificial Neural Networks, *SAJCE* (2018) in press.

Value of the data

- This data could be used by the broader scientific community as it shows the training and testing of artificial neural networks for a number of binary systems.
- Different training algorithms could be used and compared with the performance described here.
- Other computational methods and techniques could be used and compared with the data presented here.

1. Data

The data presented here is generated in preparation of a manuscript on vapour–liquid equilibrium (VLE) prediction for synthesis gas conversion using artificial neural networks (ANN) [1]. The experimental VLE data used in this study was obtained from Breman et al. [2]. Phase equilibrium modeling is a crucial element in describing the behavior of the Fischer–Tropsch (FT) reaction [3–12]. The FT reaction produces a range of hydrocarbons from light olefins and paraffins to heavy wax. Since we are comparing too many binaries to easily visualize, data for each binary is presented here. Then the summary of the overall results is published on the related paper [1]. The tables and figures presented here are unique; there is no duplication.

2. Experimental design, materials, and methods

An artificial neural network with input, hidden, and output layers was generated. The network was limited to one hidden layer and a maximum of five neurons in the hidden layer. A small network with the required accuracy is desirable for the speed of computation.

To validate the networks, the performance plots were generated for all the binary systems. The training and test curves for one representative system is presented in Fig. 1.

The performance plot does not indicate any major problems with the training. The training and test curves are very similar. If the test curves had increased significantly before the training curve increased, then it is possible that some overfitting might have occurred. The best training performance which is represented by the property tr.best_epoch indicates the iteration at which the validation performance reached a minimum. The training continued for 18 more iteration before the training stopped.

The next step is to evaluate the training state plot. The training record is used to plot the training state plot.

Another plot used to validate the network performance is the error histogram presented in Fig. 2. The error histogram plots a histogram of error values. It computes the error values as the difference between target values and predicted values, helping us to visualize the networks error.

The low values in the error histogram are an indication of a good network performance. The final step in validating the network results is by plotting a regression plot shown in Fig. 3. The solid line in the plot represents the best linear fit regression between outputs and targets.

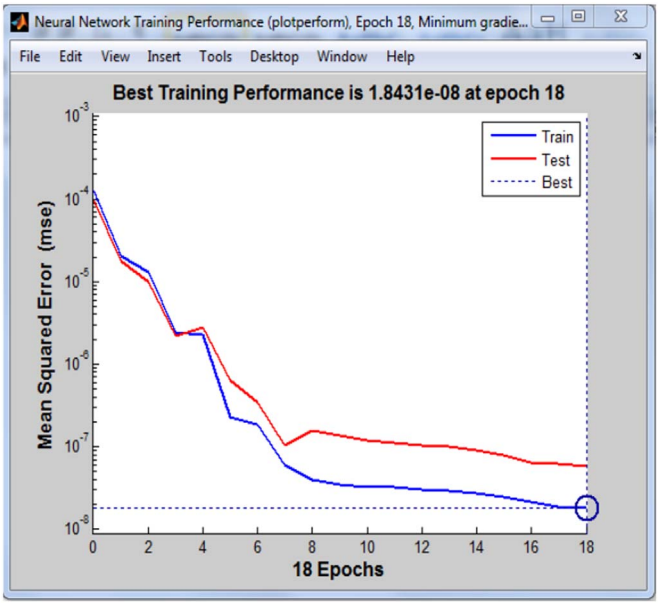

Fig. 1. Neural network performance plot.

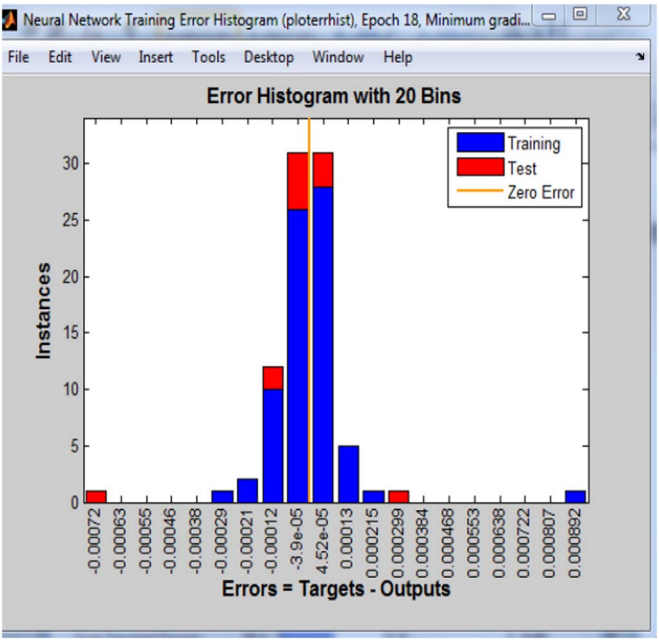

Fig. 2. Neural network error histogram.

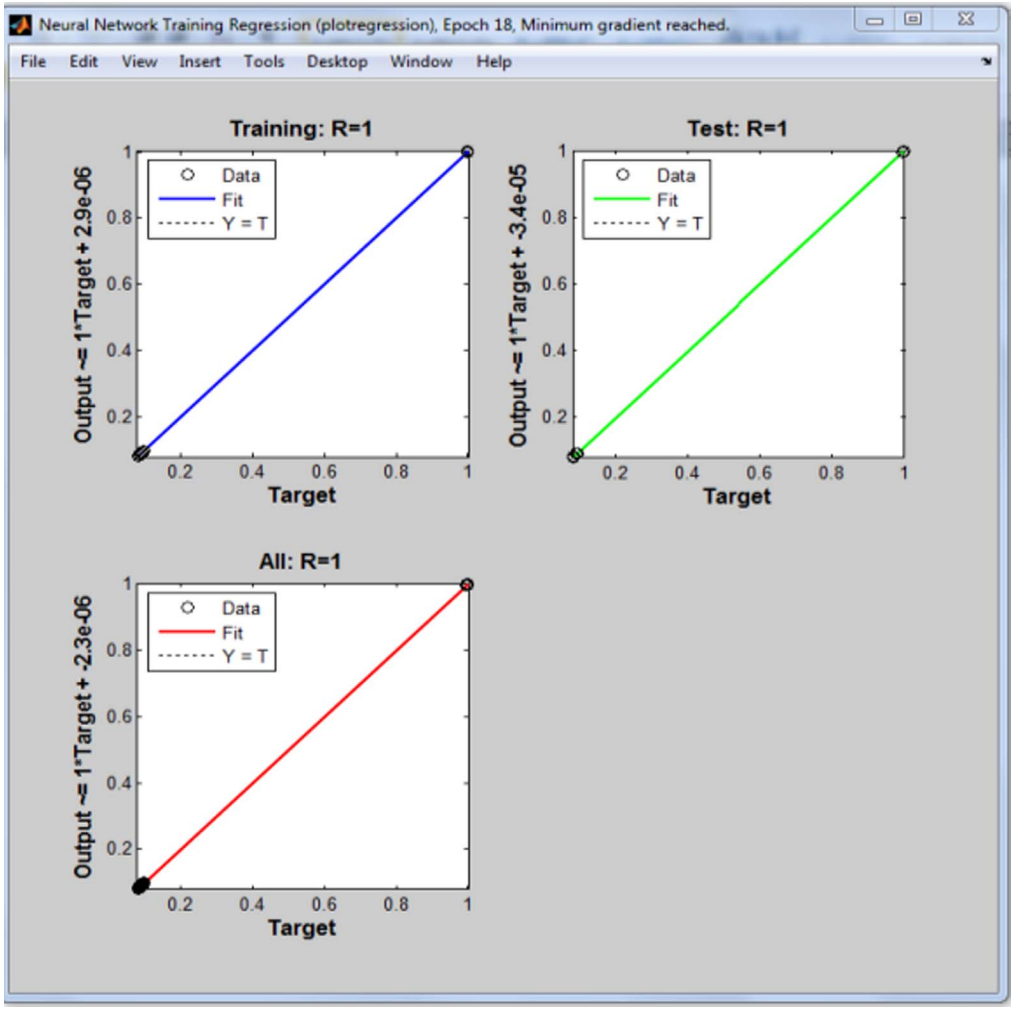

Fig. 3. Neural network regression plot.

From Fig. 3, it can be observed that training was perfect. The *R* value of 1 for the training and test data indicates that there is an exact linear relationship between our inputs and targets.

It is important to note that the plots in Figs. 1–3 were obtained after training one of the binary system, and is used to represent the plots obtained when training the entire binary system since similar plots were also obtained for each binary system.

The percentage MAE, and RMSE across each system are presented in Table 1.

The experimental values versus the predicted values for the X_i and Y_i for all the 60 binaries denoted (A1–A60) are presented in Figs. 4–15.

Table 1
%MAE and %RMSE values across each binary system.

no.	Solute	Solute	%MAE X_i	%MAE Y_i	%RMSE X_i	%RMSE Y_i
1	CO_2	$C_8H_{18}O_5$	−0.0020	0.0008	0.0210	0.0250
2	CO	$C_8H_{18}O_5$	−0.0030	−0.0102	0.0560	0.0901
3	H_2	$C_8H_{18}O_5$	0.0000	−0.0039	0.0150	0.0451
4	CH_3OH	$C_8H_{18}O_5$	−0.0260	−0.0321	0.1120	0.1235
5	C_2H_5OH	$C_8H_{18}O_5$	0.0020	−0.0005	0.0150	0.0093
6	C_3H_7OH	$C_8H_{18}O_5$	0.0007	−0.0038	0.0090	0.0154
7	C_4H_9OH	$C_8H_{18}O_5$	−0.0010	−0.0005	0.0040	0.0051
8	$C_5H_{11}OH$	$C_8H_{18}O_5$	0.0000	−0.0105	0.0080	0.1979
9	H_2O	$C_8H_{18}O_5$	0.0019	0.0001	0.0090	0.0105
10	CO_2	$C_{10}H_{14}$	0.0022	−0.0004	0.0110	0.0091
11	CO	$C_{10}H_{14}$	−0.0001	0.0007	0.0070	0.0071
12	H_2	$C_{10}H_{14}$	0.0005	−0.0005	0.0070	0.0068
13	CH_3OH	$C_{10}H_{14}$	0.0012	−0.0031	0.0040	0.0063
14	C_2H_5OH	$C_{10}H_{14}$	0.0013	−0.0017	0.0070	0.0108
15	C_3H_7OH	$C_{10}H_{14}$	0.0006	−0.0020	0.0050	0.0091
16	C_4H_9OH	$C_{10}H_{14}$	−0.0020	−0.0005	0.0210	0.0160
17	$C_5H_{11}OH$	$C_{10}H_{14}$	0.0009	−0.0014	0.0090	0.0136
18	H_2O	$C_{10}H_{14}$	−0.0050	−0.0026	0.0100	0.0090
19	CO	$C_{16}H_{34}$	−0.0008	−0.0039	0.0100	0.0158
20	H_2	$C_{16}H_{34}$	−0.0010	−0.0019	0.0310	0.0141
21	CO_2	$C_{16}H_{34}$	0.0003	0.0002	0.0100	0.0054
22	C_2H_6	$C_{16}H_{34}$	0.0002	−0.0001	0.0000	0.0052
23	C_3H_8	$C_{16}H_{34}$	0.0005	−0.0001	0.0030	0.0027
24	C_5H_{12}	$C_{16}H_{34}$	−0.0008	0.0002	0.0030	0.0043
25	C_6H_{14}	$C_{16}H_{34}$	−0.0002	−0.0003	0.0040	0.0051
26	CH_3OH	$C_{16}H_{34}$	−0.0001	−0.2533	10.030	0.4175
27	C_2H_5OH	$C_{16}H_{34}$	−0.0009	0.0009	0.0160	0.0142
28	C_3H_7OH	$C_{16}H_{34}$	0.0034	−0.0077	0.0430	0.0294
29	C_4H_9OH	$C_{16}H_{34}$	−0.0030	−0.0085	0.0110	0.0193
30	$C_5H_{11}OH$	$C_{16}H_{34}$	0.0008	−0.0014	0.0060	0.0056
31	$C_6H_{13}OH$	$C_{16}H_{34}$	−0.0030	−0.0008	0.0140	0.0091
32	H_2O	$C_{16}H_{34}$	0.0032	−0.0172	0.0790	0.1900
33	CO	$C_{16}H_{33}OH$	0.0082	−0.0005	0.0490	0.0071
34	CO_2	$C_{16}H_{33}OH$	0.0034	−0.0001	0.0260	0.0079
35	H_2	$C_{16}H_{33}OH$	−0.0010	0.0055	0.0190	0.0507
36	C_2H_6	$C_{16}H_{33}OH$	−0.0050	0.0423	0.0380	0.2254
37	C_3H_8	$C_{16}H_{33}OH$	0.0038	−0.0126	0.0090	0.0691
38	C_5H_{12}	$C_{16}H_{33}OH$	0.0012	0.0004	0.0260	0.0123
39	C_6H_{14}	$C_{16}H_{33}OH$	0.0107	0.0157	0.0870	0.2889
40	CH_3OH	$C_{16}H_{33}OH$	−0.0009	0.0001	0.0130	0.0078
41	C_2H_5OH	$C_{16}H_{33}OH$	0.0068	−0.0123	0.0740	0.2276
42	C_3H_7OH	$C_{16}H_{33}OH$	0.0007	−0.0001	0.0050	0.0146
43	C_4H_9OH	$C_{16}H_{33}OH$	0.0048	−0.0055	0.0170	0.0188
44	$C_5H_{11}OH$	$C_{16}H_{33}OH$	0.0005	0.0006	0.0040	0.0125
45	$C_6H_{13}OH$	$C_{16}H_{33}OH$	−0.0090	−0.0287	0.0140	0.0463
46	H_2O	$C_{16}H_{33}OH$	−0.0270	0.0607	0.1210	0.1731
47	CO	$C_{28}H_{58}$	−0.1100	0.0000	0.4810	0.0000
48	H_2	$C_{28}H_{58}$	0.0343	0.0000	0.2100	0.0000
49	CO_2	$C_{28}H_{58}$	0.1270	0.0000	0.5600	0.0000
50	C_2H_6	$C_{28}H_{58}$	0.0059	0.0000	0.0880	0.0000
51	C_3H_8	$C_{28}H_{58}$	0.0055	0.0000	0.0180	0.0000
52	C_5H_{12}	$C_{28}H_{58}$	0.0039	0.0000	0.0150	0.0000
53	C_6H_{14}	$C_{28}H_{58}$	0.0018	0.0000	0.0170	0.0000
54	CH_3OH	$C_{28}H_{58}$	−0.0040	0.0000	0.0200	0.0000
55	C_2H_5OH	$C_{28}H_{58}$	−0.0110	0.0000	0.0300	0.0000
56	C_3H_7OH	$C_{28}H_{58}$	0.0042	0.0000	0.1870	0.0000
57	C_4H_9OH	$C_{28}H_{58}$	−0.0030	0.0000	0.0300	0.0000
58	$C_5H_{11}OH$	$C_{28}H_{58}$	0.0059	0.0000	0.0150	0.0000
59	$C_6H_{13}OH$	$C_{28}H_{58}$	0.0002	0.0000	0.0170	0.0000
60	H_2O	$C_{28}H_{58}$	−0.0150	0.0000	0.0340	0.0000

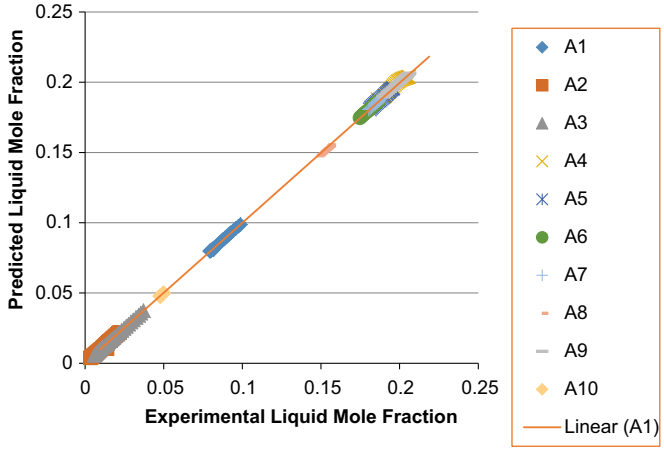

Fig. 4. Experimental Liquid Mole Fraction versus Predicted Liquid Mole fraction for system A1–A10.

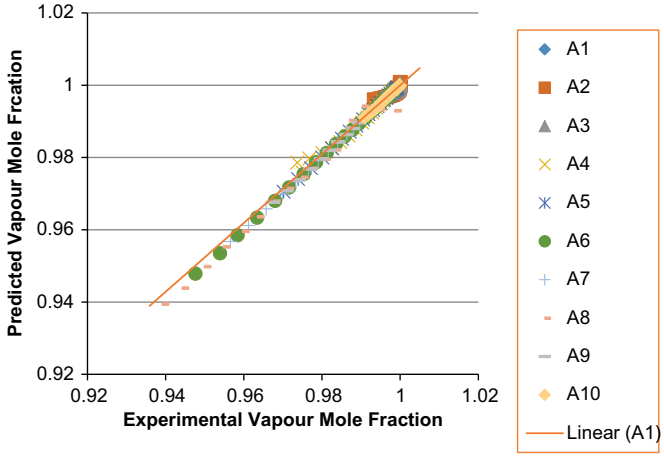

Fig. 5. Experimental Vapor Mole Fraction versus Predicted Vapor Mole fraction for system A1–A10.

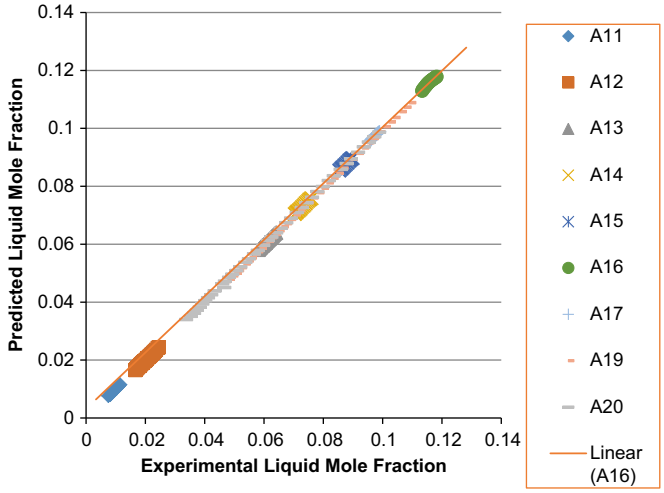

Fig. 6. Experimental Liquid Mole Fraction versus Predicted Liquid Mole fraction for system A11–A20.

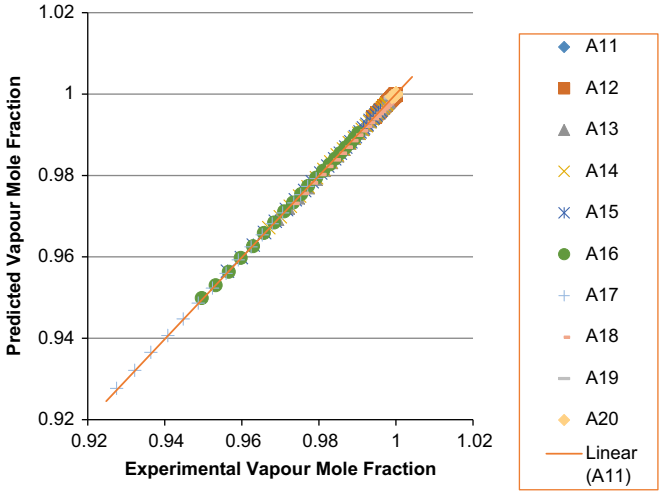

Fig. 7. Experimental Vapor Mole Fraction versus Predicted Vapor Mole fraction for system A11–A20.

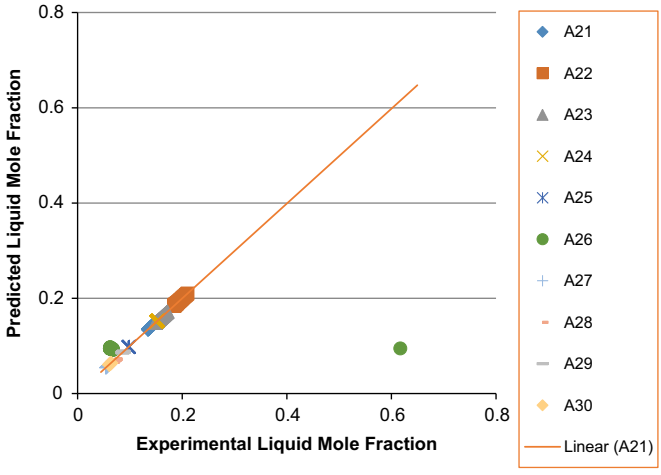

Fig. 8. Experimental Liquid Mole Fraction versus Predicted Liquid Mole fraction for system A21–A30.

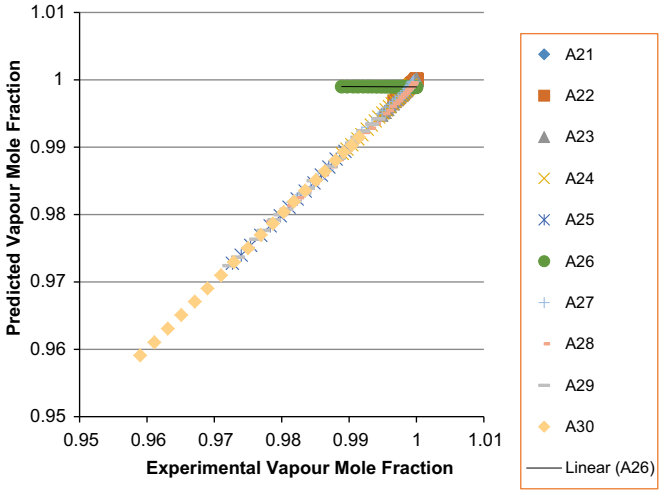

Fig. 9. Experimental Vapor Mole Fraction versus Predicted Vapor Mole fraction for system A21–A30.

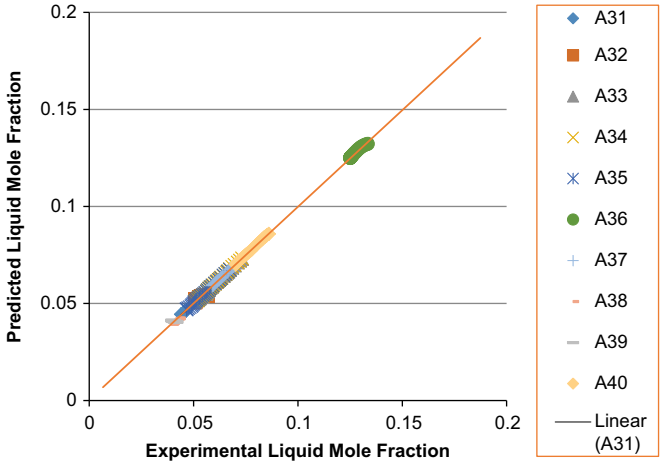

Fig. 10. Experimental Liquid Mole Fraction versus Predicted Liquid Mole fraction for system A31–A40.

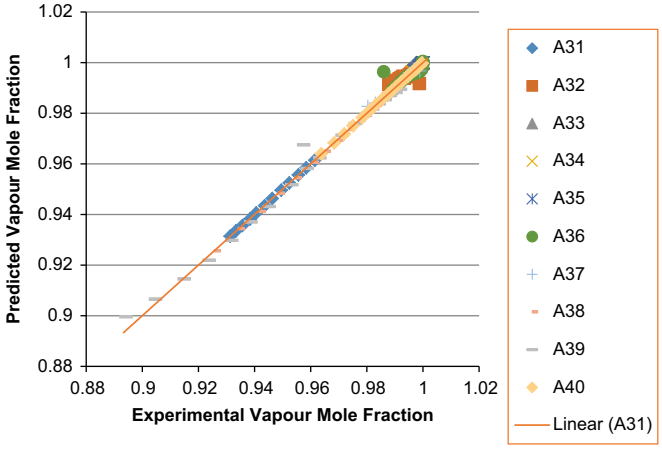

Fig. 11. Experimental Vapor Mole Fraction versus Predicted Vapor Mole fraction for system A31–A40.

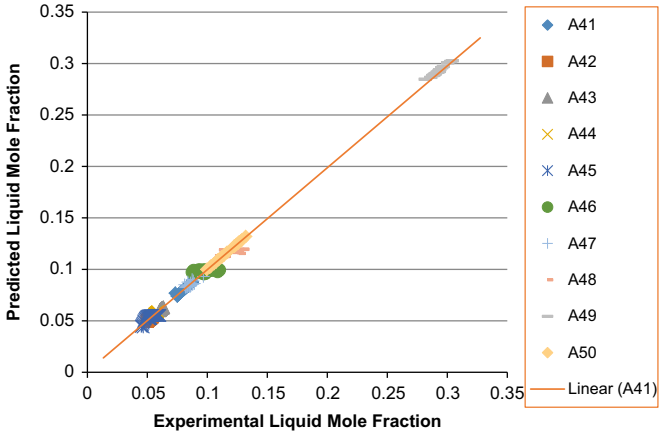

Fig. 12. Experimental Liquid Mole Fraction versus Predicted Liquid Mole fraction for system A41–A50.

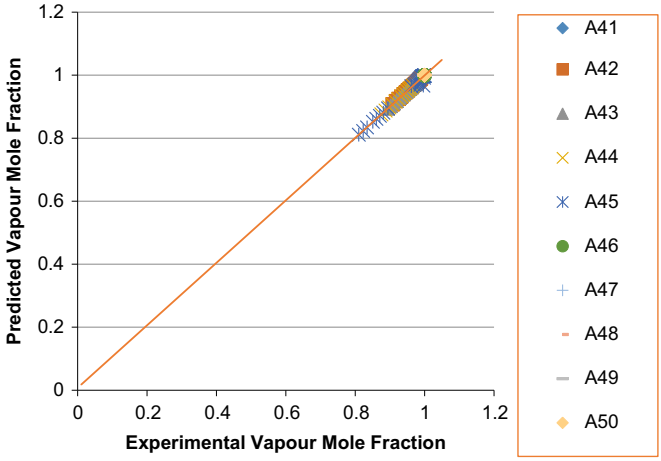

Fig. 13. Experimental Vapor Mole Fraction versus Predicted Vapor Mole fraction for system A41–A50.

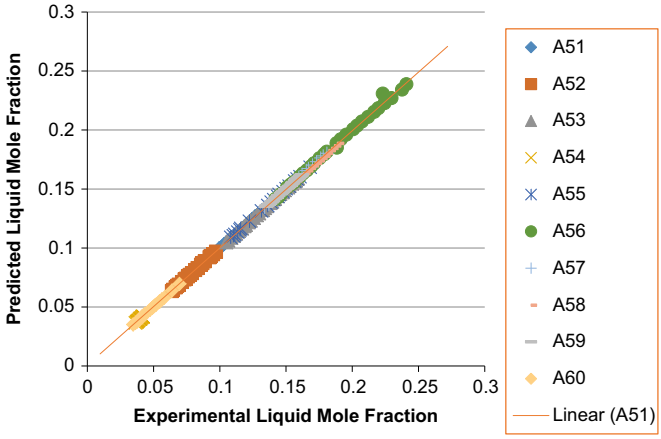

Fig. 14. Experimental Liquid Mole Fraction versus Predicted Liquid Mole fraction for system A51–A60.

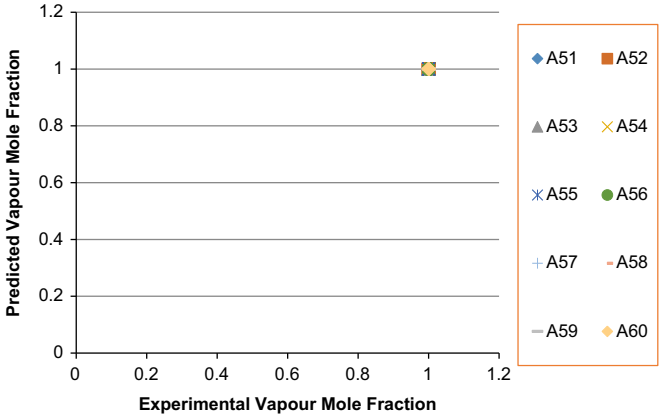

Fig. 15. Experimental Vapor Mole Fraction versus Predicted Vapor Mole fraction for system A51–A60.

Acknowledgements

We would like to acknowledge that this work has been supported in part by the National Research Foundation (NRF) of South Africa (Grant Number: 113652). The opinions, findings and conclusions/ recommendations expressed in this publication are those of the authors, and the NRF accepts no liability whatsoever in this regard.

Transparency document. Supporting information

Transparency data associated with this article can be found in the online version at https://doi.org/10.1016/j.dib.2018.10.129.

References

[1] P.C. Eze, C.M. Masuku, Vapour–liquid equilibrium prediction for synthesis gas conversion using artificial neural networks, SAJCE. *26* (2018) 80–85.
[2] B.B. Breman, A.A.C.M. Beenackers, E.W.J. Rietjens, R.J.H. Stege, Gas–liquid solubilities of carbon monoxide, carbon dioxide, hydrogen, water, 1-alcohols ($1 \leq n \leq 6$), and n-paraffins ($2 \leq n \leq 6$) in hexadecane, octacosane, 1-hexadecanol, phenanthrene, and tetraethylene glycol at pressures up to 5.5 MPa and temperatures from 293 to 553 K, J. Chem. Eng. Data *39* (1994) 647–666.
[3] L. Caldwell, D.S. van Vuuren, On the formation and composition of the liquid phase in Fischer–Tropsch reactors, Chem. Eng. Sci. *41* (1986) 89–96.
[4] B.B. Breman, A.A. Beenackers, Thermodynamic models to predict gas–liquid solubilities in the methanol synthesis, the methanol – higher alcohol synthesis, and the Fischer–Tropsch synthesis via gas–slurry processes, Ind. Eng. Chem. Res. *35* (1996) 3763–3775.
[5] C.M. Masuku, Interaction Between Reaction and Phase Equilibria in the Fischer–Tropsch Reaction (PhD Thesis), University of the Witwatersrand, 2011.
[6] C.M. Masuku, D. Hildebrandt, D. Glasser, The role of vapour–liquid equilibrium in Fischer–Tropsch product distribution, Chem. Eng. Sci. *66* (2011) 6254–6263.
[7] C.M. Masuku, W. Ma, D. Hildebrandt, D. Glasser, B.H. Davis, A vapor–liquid equilibrium thermodynamic model for a Fischer–Tropsch reactor, Fluid Phase Equilib. *314* (2012) 38–45.
[8] C.G. Visconti, Vapor–liquid equilibria in the low-temperature Fischer–Tropsch synthesis, Ind. Eng. Chem. Res. *53* (2014) 1727–1734.
[9] C.M. Masuku, X. Lu, D. Hildebrandt, D. Glasser, Reactive distillation in conventional Fischer–Tropsch reactors, Fuel Process. Technol. *130* (2015) 54–61.
[10] B.D. Kelly, A. de Klerk, Modeling vapor–liquid–liquid phase equilibria in Fischer–Tropsch syncrude, Ind. Eng. Chem. Res. *54* (2015) 9857–9869.
[11] X. Lu, X. Zhu, C.M. Masuku, D. Hildebrandt, D. Glasser, A study of the Fischer–Tropsch synthesis in a batch reactor: rate, phase of water, and catalyst oxidation, Energy Fuels *31* (2017) 7405–7412.
[12] Y. Zhang, C.M. Masuku, L.T. Biegler, Equation-oriented framework for optimal synthesis of integrated reactive distillation systems for the Fischer–Tropsch processes, Energy Fuels *32* (2018) 7199–7209.